CHEMISTRY
A EUROPEAN JOURNAL

FULL PAPER

DOI: 10.1002/chem.201303308

Triisopropylsilylethynyl-Functionalized Graphene-Like Fragment Semiconductors: Synthesis, Crystal Packing, and Density Functional Theory Calculations

Lei Zhang,[a] Alexandr Fonari,[b] Yue Zhang,[a] Guangyao Zhao,[c] Veaceslav Coropceanu,[b] Wenping Hu,[c] Sean Parkin,[d] Jean-Luc Brédas,[b] and Alejandro L. Briseno*[a]

Abstract: Tri-isopropylsilylethynyl (TIPS)-functionalized polycyclic aromatic hydrocarbon (PAH) molecules incorporate structural components of graphene nanoribbons and represent a family of model molecules that form organic crystal semiconductors for electronic devices. Here, we report a series of TIPS-functionalized PAHs and discuss their electronic properties and crystal packing features. We observe that these soluble compounds easily form one-dimensional (1D) packing arrangements and allow a direct evolution of the π stacking by varying the geometric shape. We find that the aspect ratio between length and width plays an important role on crystal packing. Our result indicates that when the PAH molecules have zigzag edges, these can provide enough volume for the molecules to rotate and reorient, alleviating the unfavorable electrostatic interactions found in perfectly cofacial π–π stacking. Density functional theory calculations were carried out to provide insights into how the molecular geometric shape influences the electronic structure and transport properties. The calculations indicate that, among the compounds studied here, "brick-layer" stacks provide the highest hole mobility.

Keywords: graphene · organic electronics · polycyclic aromatic hydrocarbon · single crystals

Introduction

In the past few decades, soluble linear acenes have been heavily studied due to their applications in organic electronic devices, such as organic field-effect transistors, and solar cells. One appealing class of molecules is based on pentacene and its derivatives, most of which exhibit excellent device performance.[1] However, oligoacenes longer than five rings are not stable due to their small ionization potentials.[2] In addition to linear acenes, two-dimensional acene analogues that represent various fragments of graphene, have also received significant attention due to their electronic properties. Molecules of this class have large, planar π surfaces that could provide increased intermolecular surface overlap. In particular, the packing of these kinds of molecules is dictated by multiple interactions that can effectively increase the dimensionality of the electronic structure, leading to enhanced transport properties.[3] A variety of two-dimensional polycyclic aromatic hydrocarbons have been synthesized and characterized by Müllen's group, such as hexa-peri-hexabenzocoronene (HBC) and its derivatives.[3a,4] In order to increase the solubility of PAHs for processing, many flexible aliphatic chains are attached to the periphery of the core structure. Some shorter side chains are favorable for self-assembling the molecules into two-dimensional arrays, which makes them suitable for photovoltaic devices.[5] However, longer side chains disrupt packing, and alkyl chains result in fewer reactive sites for further functionalization. In contrast to flexible alkyl chains, the tri-isopropylsilylethynyl (TIPS) group is a rigid spacer and it has been shown to increase the solubility, crystallinity, and stability of acenes without negatively impacting π–π interactions.[1a,b,6] For instance, TIPS-functionalized pentacene and its derivatives are now considered benchmark materials for high performance devices.

To date, only a few examples of TIPS-functionalized two-dimensional PAHs have been reported. For example, TIPS-functionalized dibenzo[*b*,*def*]chrysene was recently prepared

[a] Dr. L. Zhang, Y. Zhang, Prof. A. L. Briseno
Department of Polymer Sciences and Engineering
Conte Polymer Research Center, University of Massachusetts
Amherst, MA 01003 (USA)
Fax: (+01) 413-545-0082
E-mail: abriseno@mail.pse.umass.edu

[b] A. Fonari, Dr. V. Coropceanu, Prof. J.-L. Brédas
School of Chemistry and Biochemistry
Georgia Institute of Technology
Atlanta, Georgia, 30332 (USA)

[c] G. Zhao, Prof. W. Hu
Beijing National Laboratory for Molecular Sciences
Organic Solid Laboratory, Institute of Chemistry
Chinese Academy of Sciences, Beijing 100190 (P.R. China)

[d] Dr. S. Parkin
Department of Chemistry, University of Kentucky
Lexington, KY, 40506 (USA)

Supporting information for this article is available on the WWW under http://dx.doi.org/10.1002/chem.201303308.

and employed as an electron donor in bulk heterojunction solar cells, with efficiencies of more than 2%.[7] In a similar study, we reported 6,12-bis(tri-isopropylsilylethynyl)dibenzo-[*def*,*mno*]chrysene (TIPS–DBC) that also functions as an electron donor component in organic solar cells to yield efficiencies of approximately 2%.[8] It should be noted that most PAHs can be viewed as "pyrene derivatives," in which the change in molecular structures relative to pyrene might bring a dramatic influence on the morphological and electronic properties.[9] This molecular perspective may provide an appropriate model to better understand the relationship between the molecular structure and crystal packing. In this contribution, we present the synthesis and characterization of a series of TIPS-functionalized PAHs and provide a comparative analysis of the effect of the molecular structure on the crystal packing. This work connects fundamental principles of molecular design to crystal packing and charge transport.

Results and Discussion

Synthesis: Figure 1 shows the molecular structures of the TIPS-functionalized PAHs discussed in this study. The representative route to synthesis of the TIPS-functionalized PAHs is shown in Scheme 1. The starting materials are commercial organic dyes: isoviolanthrone, pyranthrone, anthranthrone, dibenzo[*b*,*def*]chrysene-7,14-dione, and flavathrone. Bisanthrone can be synthesized by dimerization of 3, 6-dibromo-9, 10-dihydro-9-oxoanthrance in the presence of a catalytic amount of ferrous sulfate followed by photocyclization

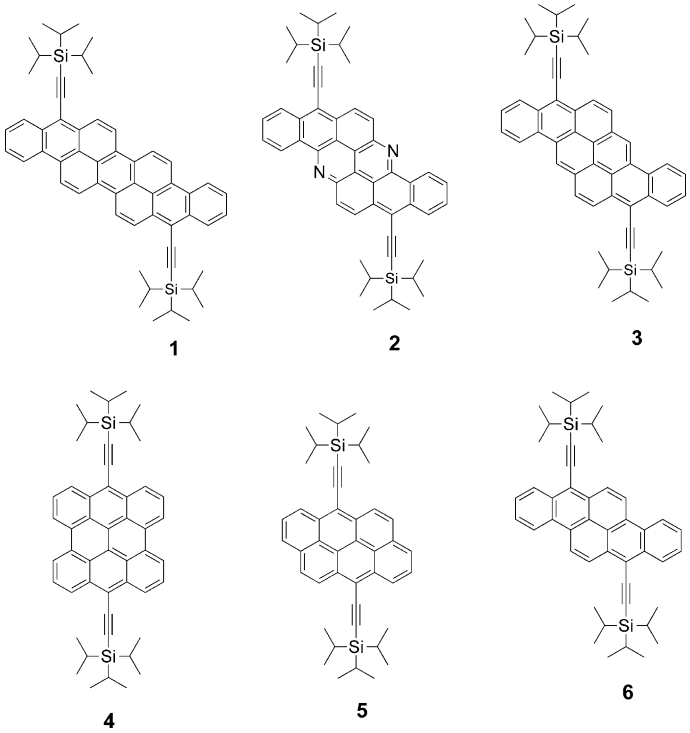

Figure 1. Molecular structures of TIPS-functionalized PAHs (**1–6**).

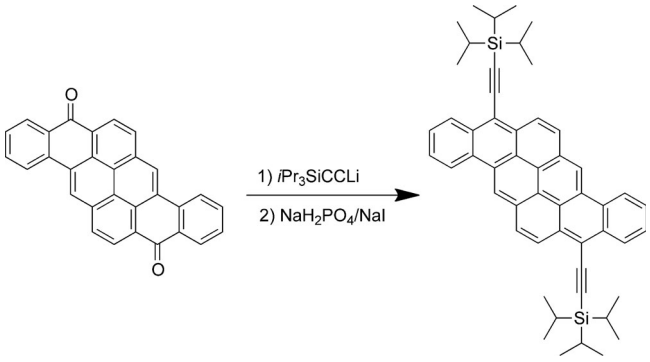

Scheme 1. Representative approaches to synthesis of TIPS-functionalized PAHs.

of the dimer.[10] Lithiation of tri-isopropylsilylacetylene in THF with BuLi to form its anion and subsequent treatment with quinones gave the relative alcohol derivatives. This was followed by a reductive aromatization with NaI/NaH$_2$PO$_4$, affording the desired products in very high yield, which were unambiguously characterized by ^{1}H NMR spectroscopy, MS, and elemental analysis. These materials are easily prepared on a large, multigram scale and are soluble in common solvents, such as THF, chloroform, toluene, and dichloromethane. They were further purified by recrystallization from hexane.

Optical spectra and cyclic voltammetry: The UV/Vis spectra of the series of TIPs functionalized PAHs were measured in chloroform solution. The experimental spectra along with the results obtained from time-dependent density functional theory (TD-DFT) calculations are shown in Figure 2 and 3. The first absorption bands of all compounds, except **4**, show a well-defined vibrational structure that can be attributed to the coupling with high-energy C–C stretching modes (about 0.15–0.20 eV). Relative to the parent unsubstituted hydrocarbons, the maximum absorption values of the present compounds exhibit a red shift of about 0.3 eV for all compounds (0.25 eV for **1**, **2**, and **6**, 0.29 eV for **3**, and 0.33 eV for **5**) except **4** that exhibits a red shift of 0.12 eV (Table 1).

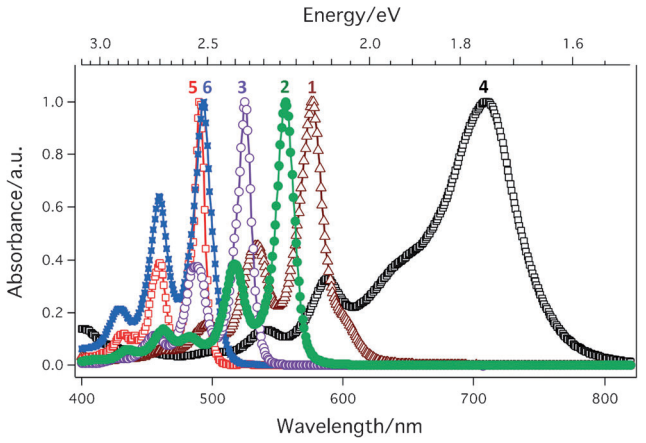

Figure 2. The absorbance spectra of **1–6** in chloroform solution.

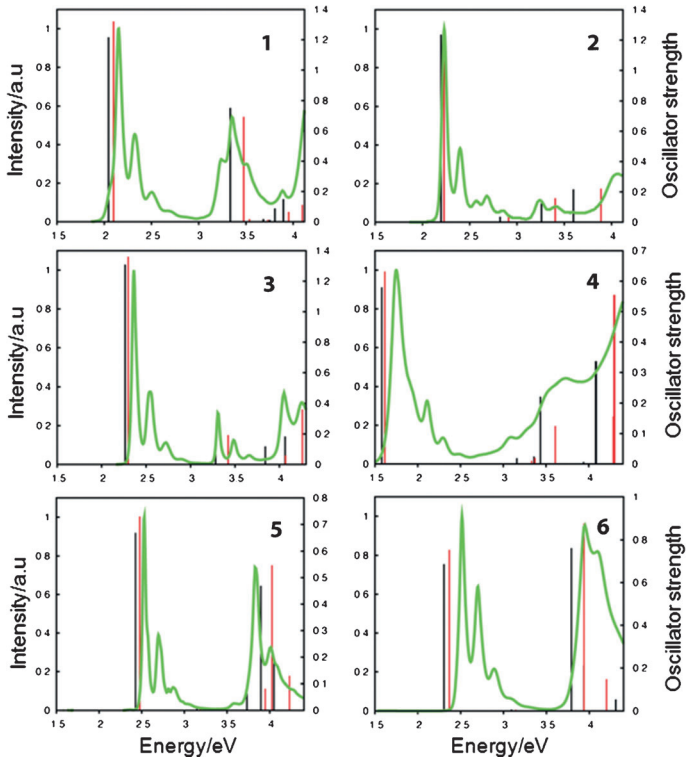

Figure 3. Experimental absorption spectra (green line) of **1–6** with transitions energies and oscillator strengths for lowest-lying states obtained from B3LYP/6-31G** (black bars) and ωB97/6-31G** (red bars) calculations.

For the sake of comparison, we note that TIPs-functionalized linear acenes show a red shift relative to their parent aromatic hydrocarbons that decreases from 0.47 to 0.14 eV when going from anthracene to pentacene.[1a,b] In general, the electronic properties of two-dimensional acenes depend on both molecular size and molecular topology (edge structure).[3] A simple interpretation of the photophysical properties of these systems can be obtained in the framework of Clar's aromatic sextet model.[15] According to Clar's sextet rule the system stability and the bandgap increases with the number of aromatic sextet rings. For instance, **5** and **6** (and their parent molecules) consist of six benzene rings and both have two sextets (see the Supporting Information); therefore, they are expected to exhibit comparable fundamental (HOMO–LUMO) gaps. Indeed the cyclic voltammetry data and the DFT results (Table 2) confirm this prediction. In addition, TD-DFT calculations reveal that the first optical band in all the present systems is described by a $S_0 \rightarrow S_1$ transition that is dominated by HOMO-to-LUMO excitation (this conclusion is also supported by the calculations of natural transition orbitals, see the Supporting Information). The TD-DFT results combined with Clar's sextet rule explain why **5** and **6** show comparable absorption bands. Molecules **3** and **4** consist of eight benzene rings; however, **3** possesses three aromatic sextets while **4** has two. As result, the energy of the S_1 state of **3** is much larger than that of **4**. It is important to note that recent studies suggest that the low gap and high energy of the HOMO in bisanthene (as is the case for periacenes in general), the parent molecule of **4**, is related to the diradical character of the ground state of this molecule arising from localized electronic states at the zigzag edges.[16] Compared with compound **3**, the absorption maximum of **2** is red shifted by 0.13 eV.[17] Molecule **1** possesses three aromatic sextets and a similar edge structure as molecule **3**; therefore, the slight redshift of the $S_0 \rightarrow S_1$ transition observed when going from **3** to **1** can be attributed to the increase in the molecular size of **1**. As seen from Figure 3, the TD-DFT calculations performed at the B3LYP/6-31G** and ωB97/6-31G** levels yield similar results and are in excellent agreement with the experimental data.

Table 1. Experimental and TD-DFT (nm eV^{-1}) $S_0 \rightarrow S_1$ transition energies in **1–6**. The experimental data for the unsubstituted molecules are also provided.

Compound	λ_{max} [exp][a]	λ_{max} [B3LYP]	λ_{max} [exp][b] unsubs.
1	575/2.13	605/2.05	521/2.38[c]
2	554/2.23	563/2.20	500/2.48[d]
3	525/2.36	547/2.26	468/2.65[e]
4	711/1.75	785/1.58	663/1.87[f]
5	490/2.53	512/2.42	434/2.86[g]
6	493/2.52	539/2.30	446/2.78[h]

[a] Measurement performed in chloroform solution. [b] The maximum absorption (λ_{max}) of parent unsubstituted molecules. [c] Isoviolanthrene, measurement performed in 1,2,4-trichlorobenzene.[11] [d] 8,16-Diazapyranthrene, measurement performed in 1,2,4-trichlorobenzene.[12] [e] Pyranthrene, measurement performed in 1,2,4-trichlorobenzene.[12] [f] Bisanthene, measurement performed in benzene 5.[13] [g] Anthanthrene, measurement performed in benzene 5.[13] [h] Dibenzo[*def*,*mno*]chrysene, measurement performed in ethanol.[14]

Table 2. Experimental estimates of the ionization potentials and B3LYP/6-31G** values of the energies (eV) of the frontier orbitals in **1–6**.

Compound	E_{IP}[a]	E_{HOMO}[b]	E_{LUMO}[b]	E_g[b]
1	−4.92	−4.67	−2.58	2.11
2	−5.36	−5.09	−2.87	2.22
3	−5.16	−4.80	−2.53	2.27
4	−4.52	−4.46	−2.86	1.60
5	−5.46	−4.90	−2.43	2.47
6	−5.45	−4.88	−2.44	2.44

[a] Determined by cyclic voltammetry (CV) in THF solution; [b] DFT results (B3LYP/6-31G**)

Cyclic voltammetry (CV) studies were performed in THF to estimate the ionization potentials (IP) of the PAHs, with 0.1 M tetrabutylammonium hexafluorophosphate ($TBAPF_6$) as the supporting electrolyte at a scan rate of 100 mV s^{-1} and onset oxidation potentials were determined relative to Fe/Fe^+ (4.8 eV). The IP values of **1–6** vary considerably with different conjugation lengths (see Table 2). Experimental and theoretical estimates of the energies of the frontier orbitals of **1–6** are also summarized in Table 2. The related frontier orbitals are shown in Figure 4. The data suggest that all the compounds are stable semiconductor materials. It is worth noting that the experimental ionization potentials of

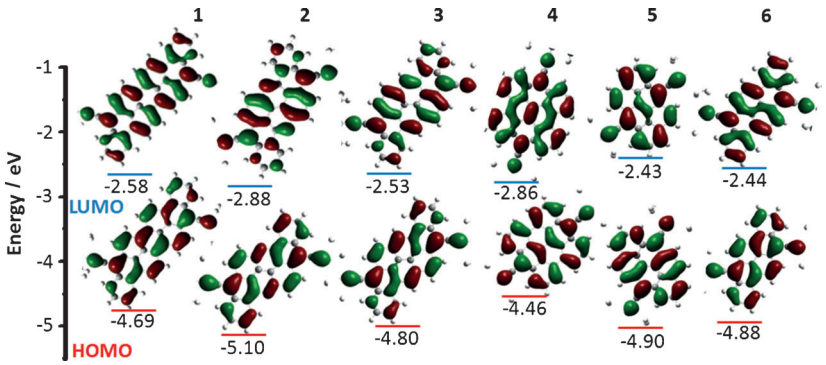

Figure 4. Frontier molecular orbitals of **1**–**6** and their energies derived by means of B3LYP/6-31G** calculations (TIPS omitted for clarity).

the compounds, except compound **4**, are in the range of the work function of the gold (1 1 1) surface (5.2 eV).[1]

Crystal packing: Generally, unsubstituted linear acenes fall into the class of herringbone packing motifs due to the dominance of C–H···π interactions in the solid state.[18] However, Anthony et al. have pointed out that TIPS groups promote linear polyacenes to crystallize in a π-stacked, more cofacial arrangement.[1a,b,6b] Compared with linear polyacenes that usually have large aspect ratios between length and width, the PAH molecules typically have comparable length and width, which has critical implications for molecular packing in the solid state.[19] However, there are limited numbers of reports on packing characterization of two dimensional molecules. This is likely due to the relative scarcity of these materials and the difficulties to obtain single crystals of sufficient size and quality. To investigate the solid-state packing of these compounds, specifically the effect of the size and shape of the aromatic cores on the packing motif, single-crystal structures for all the compounds were determined and the crystal data are summarized in Table 3.

The total aromatic core length of compound **6** is about 13.6 Å, which is comparable to that of pentacene (14 Å).[6b] As shown in Figure 5, compound **6** adopts a 2D "brickwork" arrangement with a distance of about 3.41 Å between molecules in the stacks; this distance is very similar to that of TIPS-pentacene.[6a] The difference between the crystal packings of compound **6** and TIPS-pentacene is in the intermolecular surface overlap that is about 5.64 and 7.73 Å^2 for **6** and TIPS-pentacene, respectively. It should be noted that short H···H contacts are observed between adjacent stacks in compound **6**. In contrast to **6**, compounds **4** and **5** pack in a strikingly different manner. As shown in Figure 6, **4** and **5** exhibit a 1D π-stacking motif with the tri-isopropylsilyl groups of adjacent molecules arranged in a nearly 90° alternating fashion to each other, so as to minimize steric interactions along stacks.[8] This type of intermolecular organization is reminiscent of the disc-like PAHs with flexible aliphatic chains that give rise to a one-dimensional columnar arrangement. However, compounds **4** and **5** have shorter aromatic cores (7.3 and 8.5 Å) that are probably too short to provide sufficient volume for aromatic core arrangement. This precludes slipped π–π stacks along the long axis that would form 2D stacking motif and results in a 1D packing arrangement with large π-surface overlap.

Crystals of **2** and **3** are isostructural and exhibit a 1D slipped-stack motif with similar π–π distance (3.38 Å along the *a*-axis) and π-surface overlap (18.33 Å^2). When viewed along the crystallographic *b*-axis (Figure 7), the molecules are π-stacked in two, nonequivalent stacks that are canted relative to each other. Compared with compound **6**, the presence of the two additional benzene rings on the skeleton gives rise to longer zigzag edges, which provide sufficient volume for reorientational rotation of the PAH molecules, probably due to the space-filling requirement of the bulky TIPS groups. Within a given stack, a number of H···H and C–H···π interactions between TIPS groups and cores are found. Replacement of the carbon atoms by nitrogen atoms neither changes the intermolecular interactions nor the intermolecular packing within a π-stack. However, in compound **2**, there are the H···H contacts between TIPS groups in different stacks.

Molecule **1** is almost planar and exhibits only a small amount of twist due to interactions between the core and alkynyl substituents (Figure 8). This packing pattern is very

Table 3. Summary of crystallographic data for **1**–**6**.

crystal	**1**	**2**	**3**	**4**	**5**[a]	**6**[b]	TIPS-Pen[c]
space group	$P2_1/c$	$C2/c$	$C2/c$[d]	$P\bar{1}$	$P\bar{1}$	$P\bar{1}$	$P\bar{1}$
a [Å]	19.8890 (10)	38.970 (3)	39.1798 (14)	13.7170 (7)	13.8921 (10)	8.0322 (4)	7.5647 (3)
b [Å]	7.5739 (4)	7.7845 (6)	7.7714 (2)	16.3568 (8)	15.1742 (12)	8.4306 (5)	7.7501 (3)
c [Å]	30.4514 (14)	29.422 (2)	29.5679 (8)	21.3921 (8)	35.456 (3)	16.3624 (10)	16.8354 (8)
α [°]	90.00	90.00	90.00	72.45 6 (3)	88.906 (6)	88.660 (3)	89.153
β [°]	106.665 (3)	114.726 (3)	114.893 (2)	76.756 (3)	79.711 (5)	81.815 (3)	78.421 (2)
γ [°]	90.00	90.00	90.00	73.143 (3)	84.143 (5)	61.977 (2)	83.633 (3)
π–π distance [Å]	3.40	3.34	3.38	3.29	3.40	3.41	3.47
π overlap [Å^2]	16.44	18.33	18.32	28.70	20.29	5.64	7.70

[a] ref. [8]; [b] ref. [7]; [c] ref. [6b]; [d] The deposited structure (CCDC 925865) was solved and refined using the alternative setting of *-I2/a*. Transformation to the *C*2/*c* setting makes the isostructurality of (2) and (3) much clearer.

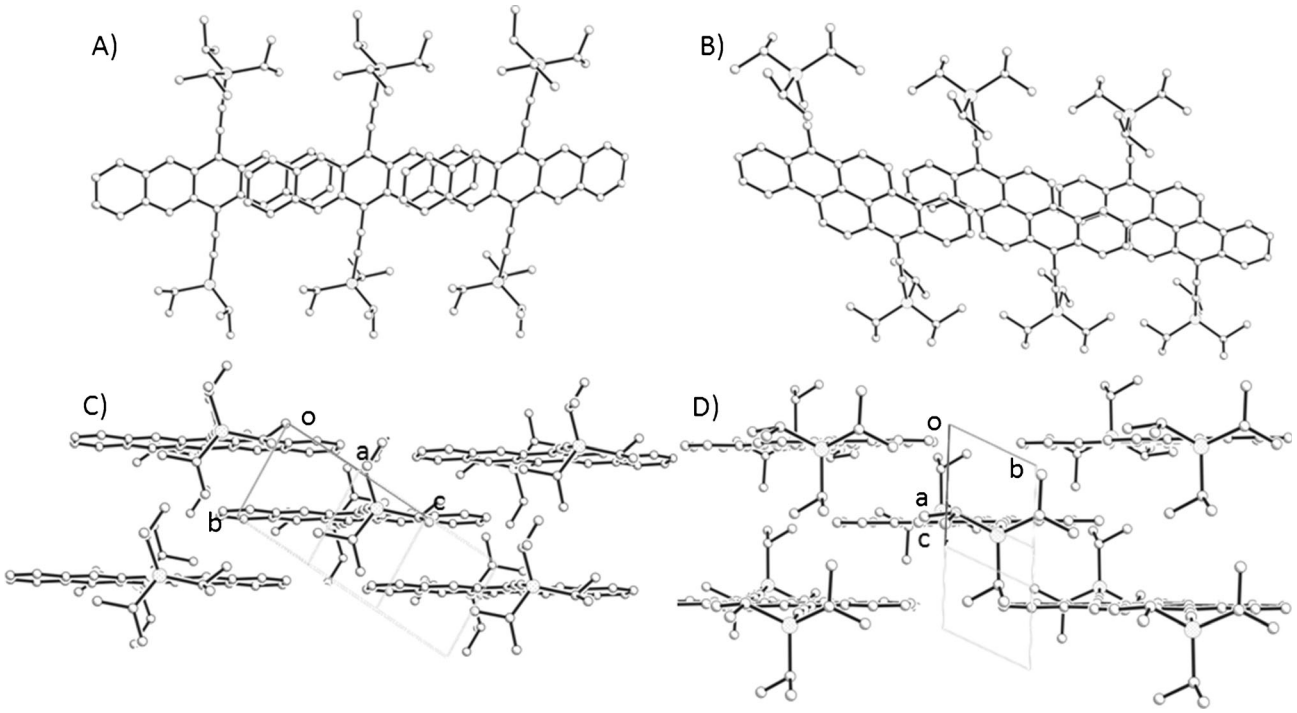

Figure 5. A) π surface overlap between stacks of TIPS-pentacene, B) π surface overlap between stacks of **6**, C) 2D packing of TIPS-pentacene, and D) 2D packing of **6**.

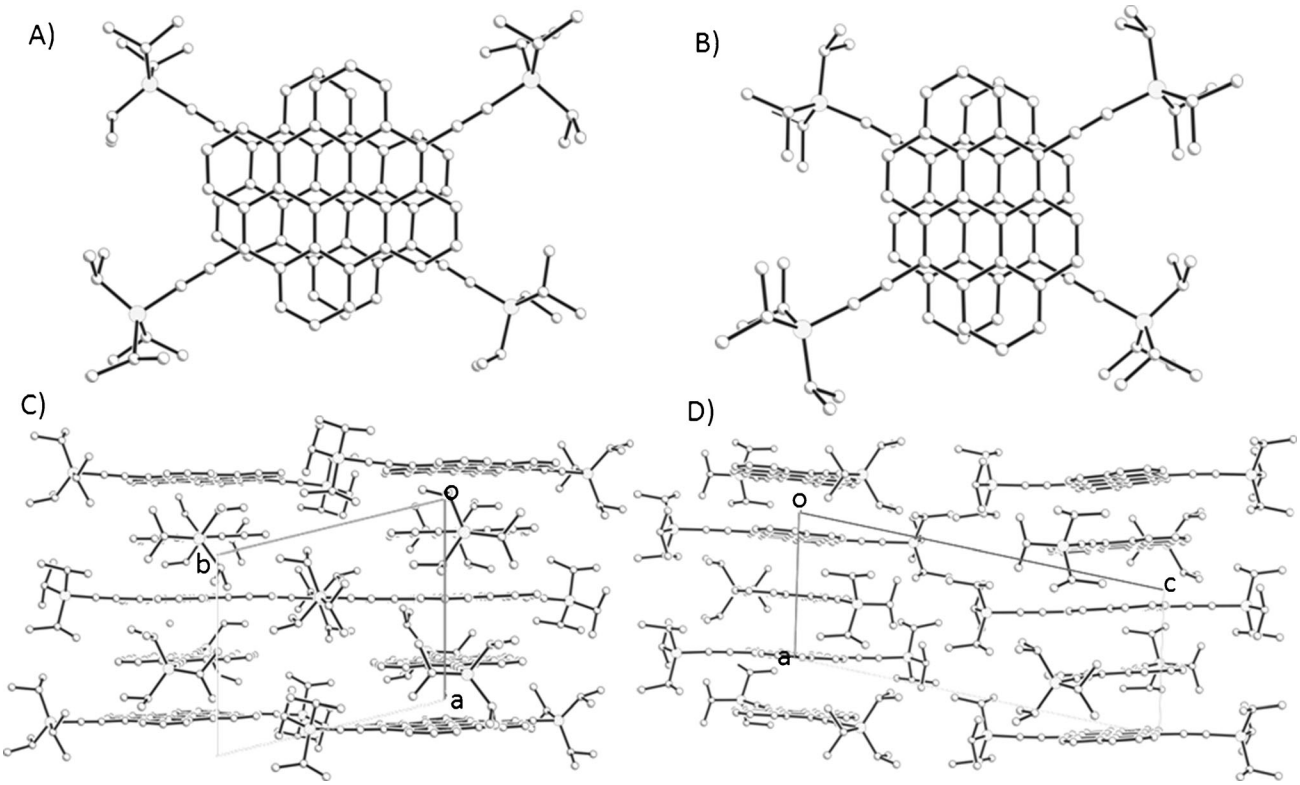

Figure 6. A) π surface overlap between stacks of **4**, B) π surface overlap between stacks of **5**, C) packing motif of **4** viewed along the *b*-axis, and D) packing motif of **5** viewed along the *c*-axis.

similar to that of compound **2**. However, there are C–H···π interactions from the cores between the different stacks due to extended π conjugation, in addition to H···H contacts from TIPS groups. These form an intricate network that binds the stacks together. The surface overlap of compound **1** is 16.44 $Å^2$, which is smaller than that of compound **3**. This

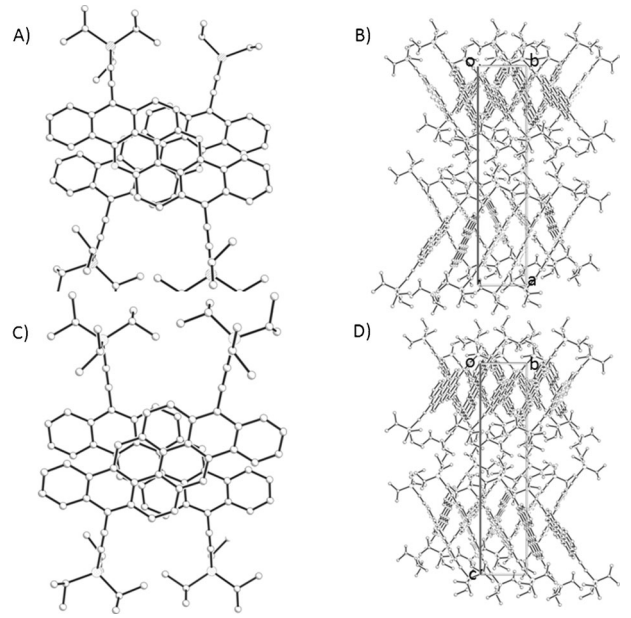

Figure 7. A) π surface overlap between stacks of **2**, B) packing motif of **2** between adjacent stacks view along *c*-axis, C) π surface overlap between stacks of **3**, and D) packing of **3** between adjacent stacks viewed along the *a*-axis.

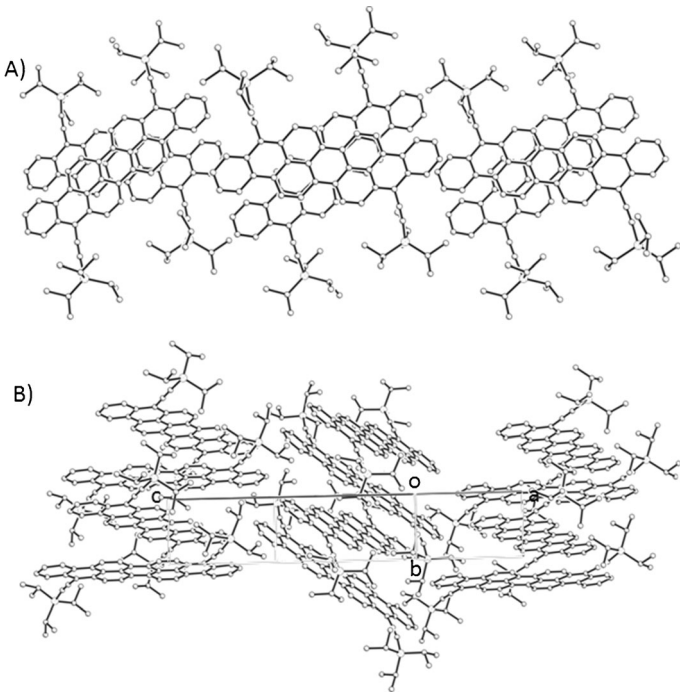

Figure 8. A) π surface overlap **1**, and B) π–π stacking between different stacks of **1**.

indicates that **1**, with its longer zigzag edge can provide enough spatial volume to minimize unfavorable steric interactions from bulky TIPS groups.

In order to study the film-forming properties of these new compounds, we deposited the materials from chloroform solution by drop-casting onto glass. All the compounds easily form large crystals with lengths from μm to mm. Compounds **2**, **3**, and **5** form needle-like crystals due to mostly one-dimensional intermolecular interactions, while compound **6** forms belt-like crystals owing to the two-dimensional packing (see the Supporting Information).

Charge-transport parameters: We turn now to a discussion of the electronic and electron-vibrational couplings, i.e., the microscopic parameters that define the charge transport properties.[20] The calculations of the electronic couplings (transfer integrals) are based on the experimental crystal geometries. The largest transfer integrals for both holes and electrons are found along the stacking directions for all systems, the related DFT estimates are listed in Table 4. The values of largest transfer integrals, *t*, for holes range from 44 meV in **5** to 194 meV in **4**. All these values are larger than that (about 30 meV) estimated at a similar level of theory for TIPS-pentacene.[21] In contrast, the values of transfer integrals for electrons that in **1**–**6** are in the range of 25–140 meV, are smaller than the value of 180 meV estimated for TIPS-pentacene.[21] We note that in **4** and **5** there are two non-equivalent dimers along the stacking directions; this is in contrast to **1**–**3** in which all dimers along a stacking direction are equivalent. The stacks in **4** and **5** are well separated by TIPS groups, which preclude electronic interactions between molecules located in different stacks. In contrast, weak inter-stack couplings (in the range of 1–9 meV) are found in **1**–**3**. Despite its 2D stacking arrangement, significant couplings in **6** are also found only along the *b*-axis. This conclusion is also supported by band-structure calculations. As seen in Figure 9, the largest bandwidth for both holes and electrons in **6** is obtained along the *b*-axis. Effective masses of approximately 0.65 m_0 and 1.4 m_0 (m_0 is the free-electron mass in vacuum) are found along this direction for holes and electrons, respectively (Figure 10). The effective masses along other directions are an order of magnitude larger. Since the unit cells of the other systems are too large to run similar calculations, we used a 1D tight binding model to estimate the effective masses of all systems along the stacking directions; the results are collected in Table 4.[22] The smallest effective mass is found for holes in **6**, 0.7 m_0, a value similar to that derived from band-structure

Table 4. The DFT estimates of the electronic coupling (*t*, meV) and the related effective masses of **1**–**6** along the stacking directions.

Crystal	hole		electron	
	t	m/m_0	*t*	$m\,m^{-1}{}_0$
1	75	3.54	86	3.08
2	75	3.36	133	1.89
3	123	2.05	140	1.80
4	−194 (143)	1.93	99 (85)	3.48
5	44 (40)	7.32	−105 (−90)	3.25
6	−78	0.69	25	2.14

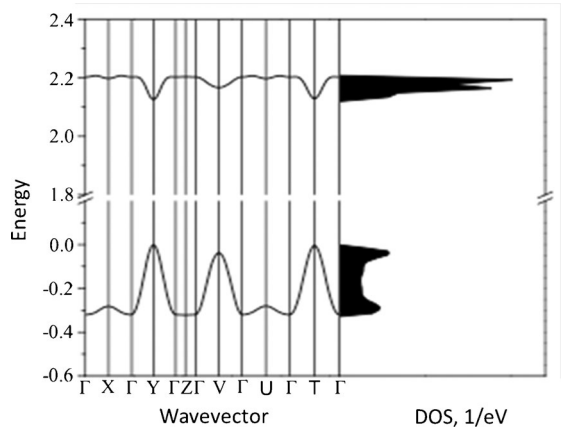

Figure 9. Calculated band structure and density of states (DOS) of **6**. The points of high symmetry in the first Brillouin zone are: $\Gamma=(0, 0, 0)$, $X=(0.5, 0, 0)$, $Y=(0, 0.5, 0)$, $Z=(0, 0, 0.5)$, $V=(0.5, 0.5, 0)$, $U=(0.5, 0, 0.5)$, $T=(0, 0.5, 0.5)$ all in crystallographic coordinates. The zero of energy corresponds to the top of the valence band.

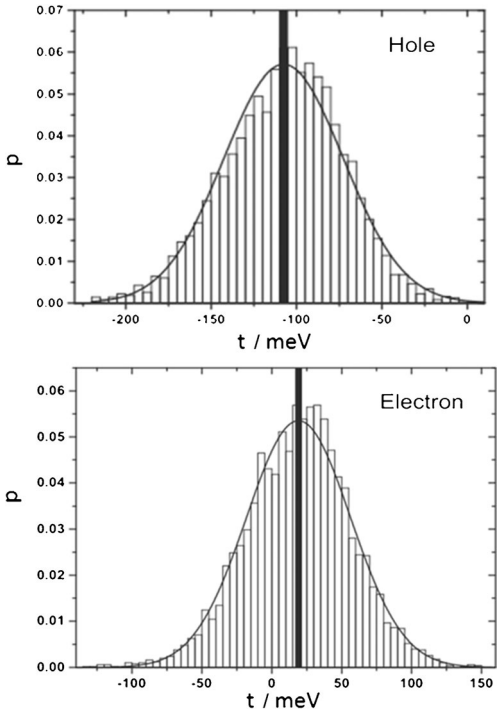

Figure 10. Normalized probability distributions of the transfer integrals for holes and electrons along the *b*-axis in **6**. The lines represent Gaussian fits and the bold vertical bars correspond to the average transfer integral, $< t >$.

calculations. In all other systems, except for holes in **5**, the effective masses of both electrons and holes are roughly 2–3 m_0.

We also investigated the local electron-vibration and hole-vibration couplings in **1**–**6**. The strength of these couplings is expressed by the polaron binding energy (E_{pol}). In context of electron-transfer theory E_{pol} is roughly equal to half the reorganization energy λ,[20] in which the reorganization energy is defined as the sum of 1) intramolecular contributions—the geometry relaxation energies upon going from the neutral to the charged-state (cation/anion) geometry and vice versa; and 2) intermolecular contributions—energy that arises from the polarization of the surrounding molecules. As the polarization contribution is expected to be small,[23] we concentrate here only on the intramolecular contribution. Calculations based on both adiabatic energy surfaces and normal-mode approaches[24] yield similar results; the results are shown in Table 5.

Table 5. Polaron binding energies E_{pol} (in meV) in **1**–**6**.

	1	**2**	**3**	**4**	**5**	**6**
Hole	77	92	83	68	83	84
Electron	104	107	112	91	111	118

For all molecules, E_{pol} is lower for holes than for electrons. The lowest value of the polaron binding energy is found in **4** for both hole and electron. The value of 68 meV for the hole E_{pol} is intermediate between the values of 48 and 72 meV derived for pentacene and TIPS-pentacene,[25] respectively. The largest value of 92 meV is found in **2**; the substitution of C–H group with a nitrogen atom when going from **3** to **2** results in an increase about 10 meV in E_{pol}. The electron E_{pol} values range from 91 meV in **4** to 118 meV in **6**. In pentacene[25] and TIPS-pentacene[26] the respective values are 66 and 102 meV. We note that the ratio of the polaron binding energy over the electronic coupling (E_{pol}/t) for holes in all the systems considered here is smaller than in TIPS-pentacene. This leads to the conclusion that the local hole-phonon coupling affects hole mobility in **1**–**6** to a lesser extent than in TIPS-pentacene. An opposite effect is found for electrons.

We note that, in addition to local electron-vibration coupling discussed here, there is a second electron-vibration mechanism referred to as the non-local coupling mechanism, that in organic molecular systems has also a strong impact on charge transport.[20] This mechanism is due to the dependence of the transfer integrals on the distances between adjacent molecules and their relative orientations. A systematic investigation of the non-local coupling would require knowledge of the phonon spectra and is beyond the scope of the present work. However, a good estimate of the overall strength of the non-local contribution can be derived by considering the variance of the transfer integrals due to thermal fluctuations, $\sigma^2=<(< t >-t)^2>$; here, $<\cdots>$ represents the average over geometrical configurations resulting from thermal motion. Using a procedure that combines molecular dynamics simulations and quantum-chemical calculations,[27] we computed the probability distribution of the transfer integrals along the *b*-axis for both electrons and holes in **6** (Figure 10). From this distribution, we then estimated σ and $< t >$. Our results show that for both holes and electrons the ratio $\sigma/< t >$ at room temperature is about 0.3.

This value is very similar to those obtained for pentacene and its derivatives, suggesting that the non-local coupling in the present systems has a similar impact on the carrier mobility as in other oligoacenes.[21,27]

The results of our electronic-structure calculations suggest large intrinsic hole mobility in **6**, with values comparable to those in pentacene and rubrene. Moderate but lower hole mobilities are expected in **1**–**3** in comparison to **6**. In the case of **4** and **5**, charge transport along stacks would in general be possible; however, the absence of electronic coupling between stacks suggests that these systems might not be suitable for application in field-effect transistor devices.

Single crystal transistors: Single crystal field-effect transistors were fabricated for compounds **1**, **2**, **5**, and **6**. The device performances of these materials are listed in Table 6.

Table 6. Device performances of single crystal transistors.

	1	**2**	**5**	**6**
μ [$cm^2V^{-1}s^{-1}$][a]	6.7×10^{-3}(2×10^{-3})	0.14 (0.06)	2.7×10^{-5}(3.6×10^{-5})	0.1 (0.05)
On/off ratio	10^3	10^4	10^3	10^3
V_{th} [V]	−5.0	−3.2	−10.0	−2.8

[a] maximum and average mobility value.

Figure 11 shows a representative output and transfer characteristic of compound **2**. Compound **3** and **4** did not exhibit appreciable mobilities because the quality of the crystals was not suitable for OFET fabrication (OFET = organic

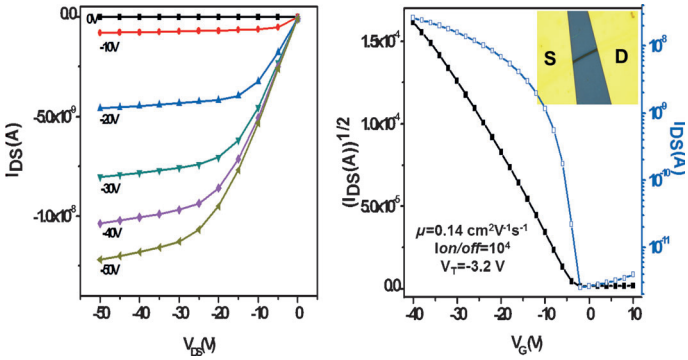

Figure 11. A representative single-crystal OFET from compound **2** showing the output and transfer characteristics.

field-effect transistor. The single crystal transistors of **2** and **6** exhibit somewhat large hole mobilities up to 0.14 and 0.1 $cm^2V^{-1}s^{-1}$, respectively. These results are in line with the theoretical calculations, although according to theory largest mobility is expected for **6**. It is noteworthy that the measured mobility of compound **6** is two orders of magnitude larger than that of the film counterpart previously reported by others.[7b]

Compound **1**, although expected to show similar transport properties as compound **2**, exhibited about one order of magnitude smaller mobilities than devices based on **2**. This discrepancy could arise, for instance, as result of a larger amount of defects in **1** due to the crystal and interface structural quality. We note that the threshold voltage in **1** is in fact larger than in **2**. Devices from compound **5** show lowest mobilities on the order of approximately 10^{-5} $cm^2V^{-1}s^{-1}$. The low mobility may be attributed to defects and, as discussed above, to poor electronic interaction between stacks.

Conclusions

We have synthesized a series of semiconductor materials based on TIPS functionalized PAH molecules by successive alteration of the molecular geometries. A comparative analysis of the packing motifs of these systems has shown that the molecular geometric shapes and intermolecular interactions have a major effect on the packing arrangement in the solid state. Edge-to-face interactions disappear in TIPS functionalized PAHs due to the bulky TIPS groups and this change often promotes packing of the PAH molecules into π–π stacks. These soluble compounds easily form one-dimensional (1D) packing arrangements due to π–π intermolecular interactions. The degree of π overlap between adjacent stacks depends on the distortions of molecules in the stack. We also observed a direct evolution of the π stacking arrangements from "cofacial" stacks to "slipped" stacks and "brick-layer" stacks by varying the geometric shape. Zigzag edges can provide enough volume for reorientational rotation of aromatic cores, alleviating the unfavorable electrostatic interactions from fully cofacial π–π stacking. This class of materials easily produces low-dimensional charge-transport systems (i.e., 1D crystals) and the single crystal transistor with compounds **2** as semiconductor material gave the mobility up to 0.14 $cm^2V^{-1}s^{-1}$. Furthermore, these zigzag-edged PAHs provide more bay regions for further functionalization and are suitable as small hydrocarbon templates for single-chirality carbon nanotubes and graphene nanoribbons.

Experimental Section

All starting materials were purchased from commercial sources and used without further purification unless there otherwise stated. THF was dried over sodium benzophenone ketyl prior to distillation under argon. The UV/Vis spectra of the homologous series of TIPS functionalized PAHs were measured in chloroform solution. The electrochemical properties of these compounds were investigated by cyclic voltammetry (CV) studies, which were performed under nitrogen in 0.1 M THF/TBAPF$_6$ solutions with a scan rate of 100 mVs^{-1}. The compounds **4**, **5**, and **6** were synthesized according to the literatures.[7,8,10a]

The molecular geometries and vibrational frequencies of the neutral and radical-ion states were derived at the DFT level. DFT calculations were performed using the B3LYP functional and the long-range corrected ωB97 functional with the 6-31G** basis set.[28] In the case of the ωB97 functional, the ω value of each molecule was optimized by minimizing

the difference between the HOMO eigenvalue of the ground state and the vertical ionization potential.[29] The optimized ω values are equal to 0.140, 0.148, 0.147, 0.152, 0.164, and 0.153 $bohr^{-1}$ for **1–6**, respectively. The TD-DFT approach was used for the evaluation of the energies of the lowest singlet excited states. To get a better insight into the nature of the $S_0 \rightarrow S_1$ transition, natural transition orbital analyses were performed following TD-DFT calculations (see the Supporting Information).[30] Transfer integrals for selected dimers of **1–6** were calculated at the DFT level by using a fragment orbital approach in combination with a basis set orthogonalization procedure.[31] All DFT calculations were performed using the Gaussian 09 package.[32] The crystal structure of **6** was optimized with the cell parameters fixed at the experimental values. The electronic band structure and density of states (DOS) were then calculated using the optimized crystal structure. These calculations were performed at the B3LYP/6-31G level with the CRYSTAL09 package.[33] The thermal fluctuations of the transfer integrals were derived by combining molecular dynamics (MD) simulations and quantum-chemical calculations. To prevent artificial symmetry effects, the supercells were initially created by a $3\times3\times3$ replication of the unit cells. The MD simulations were carried out with the Discover module of the Materials Studio package using the COMPASS force field.[34] The system was equilibrated for 150 ps using an Anderson thermostat in the NVT ensemble at 298 K and a time step of 1 fs. After equilibration, a simulation of 150 ps was run and 5000 frames were extracted by taking a snapshot every 30 fs along the trajectory. The transfer integrals for the molecular pairs taken from the MD simulation snapshots were evaluated using the ZINDO Hamiltonian.[35]

X-ray crystallographic data were collected with a Bruker-Nonius X8-Proteum rotating anode based diffractometer, using graded multilayer focused $Cu_{K\alpha}$ radiation ($\lambda = 1.54178$ Å). Data were collected at 90 K and the structures were solved by direct methods and refined by full-matrix least-squares on F^2. The computations were performed using the SHELX-97 programs. Hydrogen atoms were placed at calculated positions and refined using a riding model. CCDC 925864 (**1**), CCDC 925863 (**2**), CCDC 925865 (**3**), and CCDC 925866 (**4**) contain the supplementary crystallographic data for this paper. These data can be obtained free of charge from The Cambridge Crystallographic Data Centre via www.ccdc.cam.ac.uk/data_request/cif.

Device fabrication: The devices were fabricated by drop-casting of solutions of the compounds in toluene on SiO_2. Before the construction of the source and drain electrode, Au thin film was deposited on the SiO_2/Si substrate (please note that no Cr or Ti adhesion layer was employed to enable the removal of the Au film). Then the thin film was divided into small patterns with a mechanical probe that was manipulated with a Micromanipulator 6150 probe station. Then the small Au foil pattern was peeled off from the substrate and attached to the two ends of the crystals as electrodes. The mobility was calculated from the standard equation for saturation region: $I_{DS} = (W/2L)\mu C_i(V_G - V_T)^2$, in which I_{DS} is drain-source current, μ is field-effect mobility, W and L are the channel width and length, C_i is the capacitance per unit area of the gate insulator, V_G is the gate voltage, and V_T is the threshold voltage.

Synthesis of TIPS functionalized PAHs: To a solution of tri-isopropylsilylacetylene (5 mmol) in dry THF (250 mL), *n*BuLi (4.8 mmol) at 0 °C was added dropwise. The solution was stirred for 1 h at 0 °C before the addition of quinone (1 mmol). The mixture was warmed to room temperature and stirred overnight. The solution was then poured into water (500 mL), extracted with chloroform (200 mL), and dried over $MgSO_4$. The crude diol, NaI (10 mmol), NaH_2PO_2. H_2O (12 mmol), and acetatic acid (20 mL) was refluxed for 4 h. After cooling to room temperature, the precipitate was filtered, washed with methanol, and dried. The crude product was purified by a short silica chromatographic column.

Compound **1**: ^{1}H NMR (300 MHz, [D$_8$]THF): $\delta = 9.55$ (d, $J = 5.6$ Hz, 2H), 9.36 (dd, $J = 9.0$, 7.5 Hz, 3H), 9.19 (d, $J = 5.6$ Hz, 2H), 9.02 (dd, $J = 8.7$, 7.2 Hz, 3H), 8.87 (d, $J = 7.2$ Hz, 2H), 7.83 (t, $J = 5.2$ Hz, 4H), 1.43 ppm (m, 42H); MS (MALDI-TOF): *m/z* (%): 786.40 [M^+]; elemental analysis calcd for $C_{56}H_{68}Si_2$ (786.41): C 85.44, H 7.43; found: C 85.76, H 7.63.

Compound **2**: ^{1}H NMR (300 MHz, $CDCl_3$): $\delta = 9.10$ (d, $J = 8.2$ Hz, 2H), 8.53 (d, $J = 9.5$ Hz, 2H), 8.29 (d, $J = 8.2$ Hz, 2H), 7.94 (d, $J = 9.5$ Hz, 2H), 7.50 (t, $J = 7.2$ Hz, 2H), 7.40 (t, $J = 7.2$ Hz, 2H), 1.43 ppm (m, 42H); ^{13}C NMR (300 MHz, $CDCl_3$): $\delta = 11.73$, 19.12, 103.38, 105.69, 112.85, 117.79, 118.74, 124.12, 126.55, 126.84, 127.65, 128.93, 129.46, 129.59, 131.62, 132.09, 141.11, 148.58 ppm; MS (MALDI-TOF): *m/z* (%): 739.02 [M^+]; elemental analysis calcd for $C_{50}H_{54}N_2Si_2$ (739.15): C 82.96, H 8.23; found: C 83.31, H 8.40.

Compound **3**: ^{1}H NMR (300 MHz, $CDCl_3$): $\delta = 9.05$ (s, 2H), 8.88 (d, $J =$ 7.2 Hz, 2H), 8.77 (d, $J = 7.5$ Hz, 2H), 8.61(d, $J = 7.5$ Hz, 2H), 8.04 (d, $J =$ 9.0 Hz, 2H), 7.75 (m, 4H), 1.44 (m, 42H). MS (MALDI-TOF) *m/z* (%): 736.80 [M^+]; elemental analysis calcd for $C_{52}H_{56}Si_2$ (736.40): C 84.72, H 7.66; found: C 84.58, H 7.30.

Acknowledgements

Collaboration between the UMass and Georgia Tech groups has been supported by the Office of Naval Research under Awards N000141110636 and N000141110211. We thank Nicholas Colella for helpful discussions. S.P. acknowledges the NSF MRI program (CHE-0319176). Computational resources at Georgia Tech are supported in part by NSF under the CRIF Program (Award CHE-0946869).

[1] a) J. E. Anthony, *Angew. Chem.* **2008**, *120*, 460–492; *Angew. Chem. Int. Ed.* **2008**, *47*, 452–483; b) J. E. Anthony, *Chem. Rev.* **2006**, *106*, 5028–5048; c) J. E. Anthony, *Chem. Mater.* **2011**, *23*, 583–590; d) F. Würthner, R. Schmidt, *ChemPhysChem* **2006**, *7*, 793–797; e) M. Bendikov, F. Wudl, D. F. Perepichka, *Chem. Rev.* **2004**, *104*, 4891–4946.

[2] a) B. Purushothaman, M. Bruzek, S. R. Parkin, A. F. Miller, J. E. Anthony, *Angew. Chem.* **2011**, *123*, 7151–7155; *Angew. Chem. Int. Ed.* **2011**, *50*, 7013–7017; b) M. M. Payne, S. R. Parkin, J. E. Anthony, *J. Am. Chem. Soc.* **2005**, *127*, 8028–8029.

[3] a) J. Wu, W. Pisula, K. Müllen, *Chem. Rev.* **2007**, *107*, 718–747; b) A. K. Geim, K. S. Novoselov, *Nat. Mater.* **2007**, *6*, 183–191; c) Z. Sun, Q. Ye, C. Chi, J. Wu, *Chem. Soc. Rev.* **2012**, *41*, 7857–7889.

[4] a) M. D. Watson, A. Fechtenkötter, K. Müllen, *Chem. Rev.* **2001**, *101*, 1267–1300; b) A. J. Berresheim, M. Müller, K. Müllen, *Chem. Rev.* **1999**, *99*, 1747–1786.

[5] a) W. Pisula, Ž. Tomović, C. Simpson, M. Kastler, T. Pakula, K. Müllen, *Chem. Mater.* **2005**, *17*, 4296–4303; b) L. Schmidt-Mende, A. Fechtenkötter, K. Müllen, E. Moons, R. H. Friend, J. D. Mackenzie, *Science* **2001**, *293*, 1119–1122.

[6] a) S. Subramanian, S. K. Parkin, J. E. Anthony, V. Podzorov, T. N. Jackson, J. E. Anthony, *J. Am. Chem. Soc.* **2008**, *130*, 2706–2707; b) J. E. Anthony, D. L. Eaton, S. R. Parkin, *Org. Lett.* **2001**, *4*, 15–18; c) O. Tverskoy, F. Rominger, A. Peters, H. J. Himmel, U. H. F. Bunz, *Angew. Chem.* **2011**, *123*, 3619–3622; *Angew. Chem. Int. Ed.* **2011**, *50*, 3557–3560; d) S. Miao, S. M. Brombosz, P. V. R. Schleyer, J. I. Wu, S. Barlow, S. R. Marder, K. I. Hardcastle, U. H. F. Bunz, *J. Am. Chem. Soc.* **2008**, *130*, 7339–7344; e) B. D. Lindner, J. U. Engelhart, O. Tverskoy, A. L. Appleton, F. Rominger, A. Peters, H. J. Himmel, U. H. F. Bunz, *Angew. Chem.* **2011**, *123*, 8747–8750; *Angew. Chem. Int. Ed.* **2011**, *50*, 8588–8591; f) A. L. Appleton, S. M. Brombosz, S. Barlow, J. S. Sears, J. L. Brédas, S. R. Marder, U. H. F. Bunz, *Nat. Commun.* **2010**, *1*, 1–6; g) U. H. F. Bunz, *Chem. Eur. J.* **2009**, *15*, 6780–6789; h) S. Miao, A. L. Appleton, N. Berger, S. Barlow, S. R. Marder, K. I. Hardcastle, U. H. F. Bunz, *Chem. Eur. J.* **2009**, *15*, 4990–4993.

[7] a) K. N. Winzenberg, P. Kemppinen, G. Fanchini, M. Bown, G. E. Collis, C. M. Forsyth, K. Hegedus, T. B. Singh, S. E. Watkins, *Chem. Mater.* **2009**, *21*, 5701–5704; b) K. B. Burker, Y. Shu, P. Kemppinen, B. Singh, M. Bown, I. I. Liaw, R. M. Williamson, L. Thomsen, P. Dastoor, W. Belcher, C. Forsyth, K. N. Winzenberg, G. E. Collis, *Cryst. Growth Des.* **2012**, *12*, 725–731.

[8] L. Zhang, B. Walker, F. Liu, N. S. Colella, S. C. B. Mannsfeld, J. J. Watkins, T. Q. Nguyen, A. L. Briseno, *J. Mater. Chem.* **2012**, *22*, 4266–4268.
[9] T. M. Figueira-Duarte, K. Müllen, *Chem. Rev.* **2011**, *111*, 7260–7314.
[10] a) J. Li, K. Zhang, X. Zhang, K. W. Zhang, C. Chi, J. Wu, *J. Org. Chem.* **2010**, *75*, 856–863; b) J. Li, C. Jiao, K. W. huang, J. Wu, *Chem. Eur. J.* **2011**, *17*, 14672–14680; c) E. H. Fort, P. M. Donovan, L. T. Scott, *J. Am. Chem. Soc.* **2009**, *131*, 16006–16007.
[11] S. Iwashima, T. Ueda, H. Honda, T. Tsujioka, M. Ohno, J. Aoki, T. Kan, *J. Chem. Soc. Perkin Trans. 1* **1984**, 2177–2178.
[12] J. Aoki, *Bull. Chem. Soc. Jpn.* **1968**, *41*, 1017–1020.
[13] J. B. Birks, *Photophysics of Aromatic Molecules*, Wiley-Interscience, London, **1970**.
[14] R. G. Harvey, J. Pataki, C. Cortez, P. Di Raddo, C. X. Yang, *J. Org. Chem.* **1991**, *56*, 1210–1217.
[15] E. Clar, *The Aromatic Sextet*, Wiley, New York, **1972**.
[16] D. Jiang, B. G. Sumpter, S. Dai, *J. Chem. Phys.* **2007**, *127*, 124703.
[17] Z. Liang, Q. Tang, R. Mao, D. Liu, J. Xu, Q. Miao, *Adv. Mater.* **2011**, *23*, 5514–5518.
[18] a) M. D. Curtis, J. Cao, J. W. Kampf, *J. Am. Chem. Soc.* **2004**, *126*, 4318–4328; b) G. R. Desiraju, A. Gavezzotti, *Acta Crystallogr. B* **1988**, *44*, 427–434.
[19] a) J. C. Zhong, M. Munakata, T. Kuroda-Sowa, M. Maekawa, Y. Suenaga, H. Konaka, *Inorg. Chem.* **2001**, *40*, 3191–3199; b) L. Zhang, S. M. Fakhouri, F. Liu, J. C. Timmons, N. A. Ran, A. L. Briseno, *J. Mater. Chem.* **2011**, *21*, 1329–1377; c) L. Zhang, L. Tan, Z. H. Wang, W. P. Hu, D. B. Zhu, *Chem. Mater.* **2009**, *21*, 1993–1999; d) L. Zhang, L. Tan, W. P. Hu, Z. H. Wang, *J. Mater. Chem.* **2009**, *19*, 8216–8222; e) L. Tan, L. Zhang, X. Jiang, X. D. Yang, L. J. Wang, Z. H. Wang, L. Q. Li, W. P. Hu, Z. G. Shui, L. Lin, D. B. Zhu, *Adv. Funct. Mater.* **2009**, *19*, 272–276.
[20] V. Coropceanu, J. Cornil, D. A. da Silva Filho, Y. Olivier, R. Silbey, J. L. Brédas, *Chem. Rev.* **2007**, *107*, 926–952.
[21] A. Troisi, G. Orlandi, J. E. Anthony, *Chem. Mater.* **2005**, *17*, 5024–5031.
[22] S. Salman, M. C. R. Delgado, V. Coropceanu, J. L. Brédas, *Chem. Mater.* **2009**, *21*, 3593–3601.
[23] a) J. E. Norton, J. L. Brédas, *J. Am. Chem. Soc.* **2008**, *130*, 12377–12384; b) N. G. Martinelli, Y. Olivier, S. Athanasopoulos, M. C. Ruiz-Delgado, K. R. Pigg, D. A. da Silva, R. S. Sánchez-Carrere, E. Venuti, R. G. D. Valle, J. L. Brédas, D. Beljonne, J. Cornil, *ChemPhysChem* **2009**, *10*, 2265–2273.
[24] M. Malagoli, V. Coropceanu, D. A. D. S. Filho, J. L. Brédas, *J. Chem. Phys.* **2004**, *120*, 7490–7496.
[25] a) V. Coropceanu, M. Malagoli, D. A. da Silva, N. E. Gruhn, T. G. Bill, J. L. Brédas, *Phys. Rev. Lett.* **2002**, *89*, 275503; b) N. E. Gruhn, D. A. da Silva, T. G. Bill, M. Malagoli, V. Coropceanu, A. Kahn, J. L. Brédas, *J. Am. Chem. Soc.* **2002**, *124*, 7918–7919.
[26] C. H. Li, C. H. Huang, M. Y. Kuo, *Phys. Chem. Chem. Phys.* **2011**, *13*, 11148–11155.
[27] a) M. C. R. Delgado, K. R. Pigg, D. A. D. S. Fiho, N. E. Gruhn, Y. Sakamoto, T. Suzuki, R. M. Osuna, J. Casado, V. Hernandez, J. T. L. Navarrete, N. G. Martinelli, J. Cornil, R. S. Sanchez-Carrera, V. Coropceanu, J. L. Brédas, *J. Am. Chem. Soc.* **2009**, *131*, 1502–1512; b) A. Troisi, G. Orlandi, *J. Phys. Chem. A* **2006**, *110*, 4065–4070; c) Y. P. Yi, V. Coropceanu, J. L. Brédas, *J. Chem. Phys.* **2012**, *137*, 164303.
[28] J. Chai, M. J. Head-Gordon, *J. Chem. Phys.* **2008**, *128*, 084106–15.
[29] T. Stein, H. Eisenberg, L. Kronik, R. Baer, *Phys. Rev. Lett.* **2010**, *105*, 266802.
[30] R. L. Martin, *J. Chem. Phys.* **2003**, *118*, 4775–4777.
[31] E. F. Valeev, V. Coropceanu, D. A. da Silva Filho, S. Salman, J. L. Brédas, *J. Am. Chem. Soc.* **2006**, *128*, 9882–9886.
[32] Gaussian 09, Revision B.01, M. J. Frisch, G. W. Trucks, H. B. Schlegel, G. E. Scuseria, M. A. Robb, J. R. Cheeseman, G. Scalmani, V. Barone, B. Mennucci, G. A. Petersson, H. Nakatsuji, M. Caricato, X. Li, H. P. Hratchian, A. F. Izmaylov, J. Bloino, G. Zheng, J. L. Sonnenberg, M. Hada, M. Ehara, K. Toyota, R. Fukuda, J. Hasegawa, M. Ishida, T. Nakajima, Y. Honda, O. Kitao, H. Nakai, T. Vreven, J. A. Montgomery, J. E. Peralta, F. Ogliaro, M. Bearpark, J. J. Heyd, E. Brothers, K. N. Kudin, V. N. Staroverov, R. Kobayashi, J. Normand, K. Raghavachari, A. Rendell, J. C. Burant, S. S. Iyengar, J. Tomasi, M. Cossi, N. Rega, J. M. Millam, M. Klene, J. E. Knox, J. B. Cross, V. Ballen, C. Adamo, J. Jaramillo, R. Gomperts, R. E. Stratmann, O. Yazyev, A. J. Austin, R. Cammi, C. Pomelli, J. W. Ochterski, R. L. Martin, K. Morokuma, V. G. Zakrzewski, G. A. Voth, P. Salvador, J. J. Dannenberg, S. Dapprich, A. D. Daniels, J. B. Foresman, J. V. Ortiz, J. Cioslowski, D. J. Fox, Wallingford CT, **2009**.
[33] V. R. Saunders, R. Dovesi, C. Roetti, R. Orlando, C. M. Zicovich-Wilson, N. M. Harrison, K. Doll, B. Civalleri, I. J. Bush, P. D′Arco, M. Llunell, *CRYSTAL09 User's Manual*; Torino, Italy, **2009**.
[34] S. W. Bunte, H. Sun, *J. Phys. Chem. B* **2000**, *104*, 2477–2489.
[35] J. Ridley, M. Zemer, *Theor. Chim. Acta* **1973**, *32*, 111–134.

Received: August 23, 2013
Published online: November 25, 2013

